(Preprint) AAS 16-317

INTRODUCING A DEGREE OF FREEDOM IN THE FAMILY OF GENERALIZED LOGARITHMIC SPIRALS

Javier Roa*and Jesús Peláez†

The versatility of the family of generalized logarithmic spirals is improved by introducing a degree of freedom in the solution. The low-thrust acceleration profile now includes a control term that affects both the magnitude and the direction of the thrust. Exact and fully analytic solutions to the trajectory, the velocity, the time of flight, *etc*. are made available. Two integrals of motion are preserved. The first one is a generalization of the equation of the energy and depends on the values of the control parameter. The second one relates to the equation of the angular momentum. The problem of finding spiral transfers between two arbitrary state vectors reduces to solving one algebraic equation with one unknown. The degree of freedom allows fixing the time of flight of the transfer. If the time of flight is fixed, then there are two equations with two unknowns. No other iterative procedures are required. Coast arcs can be introduced in the solution naturally. An explicit expression for the maximum acceleration reached along the transfer is provided. Thanks to the symmetry properties of the solution a simple algorithm for generating periodic orbits is presented. An arbitrary number of intermediate nodes can be introduced to improve the flexibility of the solution when facing optimization problems. An example of a low-thrust gravity-assist Earth-Mars-Ceres trajectory shows that the solution is comparable to that obtained with other preliminary design techniques.

INTRODUCTION

Generating an adequate initial guess for low-thrust trajectory optimization is a critical task. The optimizer requires a sufficiently good seed in order to converge to an optimal. Providing an initial guess for the indirect method is particularly difficult since the costates need to be initialized but they lack an intuitive or physical interpretation.

Prior to the optimization phase the space of solutions is explored using simplified methods. These preliminary design techniques are not conceived to find the optimal solution, but rather to bound the intervals in which the accurate search will be carried out. Shape-based methods have been widely applied to preliminary low-thrust mission design. The trajectory is assumed to have a certain shape and the design problem reduces to adjusting a number of shape coefficients. This method dates back to the 50's, when Bacon[1] and Tsu[2] found the thrust required to follow a logarithmic spiral. Petropoulos and Longuski[3] proposed a more flexible curve, the exponential sinusoid, that they implemented into an automatic mission design tool including gravity-assist maneuvers. Pascale and

*PhD Candidate, Space Dynamics Group, Technical University of Madrid, Pza. Cardenal Cisneros 3, 28040, Madrid. Student Member AIAA. javier.roa@upm.es

Present address: Jet Propulsion Laboratory, California Institute of Technology, 4800 Oak Grove Drive, Pasadena, CA 91109-8099, USA

†Professor and Head, Space Dynamics Group, Technical University of Madrid, Pza. Cardenal Cisneros 3, 28040, Madrid. Member AIAA.

Vasile[4] introduced the pseudo-equinoctial elements for mission design. Gondelach and Noomen[5] proposed a different approach based on the definition of the trajectory in the space of velocities.

Analytic solutions are the core of preliminary trajectory design methods. Different authors have explored specific thrust profiles looking for closed-form solutions. Variants of the constant radial thrust problem are good examples. Originally formulated by Tsien[6] in 1953, it has been recently revisited be Izzo and Biscani[7] and by Urrutxua *et al.*[8] The former introduced the Weierstrass functions whereas the latter solved the problem with the Dromo formulation.[9,10,11] An interesting property of the radial thrust problem is the conservation of two integrals of motion. This allows following an energy-driven approach and simplifies the interpretation of the solutions.[12]

Roa and Peláez[13,14] combined these three elements into a novel method: the design process reduces to adjusting some shape coefficients, the motion is completely solved in closed-form (including the time of flight), and there are two first integrals. They referred to this new solution as the family of generalized logarithmic spirals, because the thrust profile is that used by Bacon to render logarithmic spirals. The family is classified in elliptic, parabolic and hyperbolic spirals by means of the constant of the generalized energy. In this paper we extend the flexibility of this solution by introducing a control parameter, which yields an additional degree of freedom. This overcomes the limitations of the method reported in the original papers, like the need of impulsive maneuvers in order to leave a circular orbit. The result is a fully analytic solution, physically intuitive thanks to the conserved quantities, and capable of finding preliminary solutions like the ones generated with previous methods. Advantages with respect to them are the fact that the time of flight is solved analytically and that the trajectory admits constraints on the initial and final velocities simultaneously.

The paper is organized as follows. The next section formulates the equations of motion. In the following three sections the problem is solved for the case of elliptic, parabolic and hyperbolic spirals. Then spiral transfers between arbitrary state vectors are solved, and a method for generating periodic orbits is presented. Finally we solve an example of a low-thrust transfer from the Earth to Ceres with a gravity-assist maneuver at Mars.

EQUATIONS OF MOTION

Consider the motion of a particle in a central gravity field with $\mu = 1$ and perturbed by a thrust acceleration of the form:

$$\mathbf{a}_\mathrm{p} = \frac{1}{r^2}(\xi \cos\psi\, \mathbf{t} + \eta \sin\psi\, \mathbf{n}) \tag{1}$$

where ξ and η are constants that behave as control parameters, and ψ is the flight-direction angle. The angle between the radial direction and the thrust vector will be denoted α. The acceleration $\mathbf{a}_\mathrm{p}$ is written in the intrinsic frame $\mathcal{T} = \{\mathbf{t}, \mathbf{n}, \mathbf{b}\}$. Frame $\mathcal{T}$ is defined by the basis

$$\mathbf{t} = \frac{\mathbf{v}}{v}, \qquad \mathbf{b} = \frac{\mathbf{r}\times\mathbf{v}}{rv}, \qquad \mathbf{n} = \mathbf{b}\times\mathbf{t}$$

Setting $\xi = 1/2$ and $\eta = 0$ in Eq. (1) defines the tangential thrust profile that originated the family of generalized logarithmic spirals.[13,14] The case $\xi = 0$ and $\eta = 0$ corresponds to Kepler's problem. Combining this thrust profile with the gravitational acceleration

$$\mathbf{a}_\mathrm{g} = -\frac{1}{r^2}(\cos\psi\, \mathbf{t} - \sin\psi\, \mathbf{n})$$

yields the equations of motion projected on the intrinsic frame:

$$\frac{\mathrm{d}v}{\mathrm{d}t} = \frac{\xi - 1}{r^2}\cos\psi \tag{2}$$

$$v\frac{\mathrm{d}}{\mathrm{d}t}(\psi + \theta) = \frac{1 + \eta}{r^2}\sin\psi \tag{3}$$

$$\frac{\mathrm{d}r}{\mathrm{d}t} = v\cos\psi \tag{4}$$

$$\frac{\mathrm{d}\theta}{\mathrm{d}t} = \frac{v}{r}\sin\psi \tag{5}$$

In the limit case $\xi \to 1$ the thrust compensates the gravitational attraction of the central body and the velocity remains constant. We consider this a natural limit to the control parameter, so $\xi < 1$. The control parameters ξ and η can be bounded from limitations on the local ratio between the thrust acceleration and the gravitational attraction. Figure 1 sketches the geometry of the problem.

Equation (4) defines the radial velocity in terms of the flight-direction angle and determines the *regime* of the trajectory. The spiral is said to be in raising regime if it is traveling away from the center of attraction, $\dot{r} > 0$. In this case it is $\psi \in (0, \pi/2)$ and $\cos\psi > 0$. If the spiral is approaching the center of attraction, $\dot{r} < 0$, it is in lowering regime. This yields $\psi \in (\pi/2, \pi)$ and $\cos\psi < 0$. The limits $\psi = 0$ and $\psi = \pi$ are omitted since they correspond to degenerate rectilinear orbits. When considering orbit transfers between two given points the transfer is called *direct* if there are no transitions between regimes. Conversely, for *indirect* trajectories the spiral transitions between regimes during the transfer.

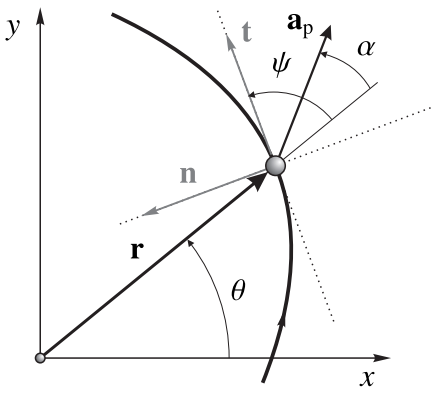

Figure 1: **Geometry of the problem**

Dividing Eqs. (2) and (4) provides

$$\frac{\mathrm{d}v}{\mathrm{d}r} = \frac{\xi - 1}{r^2 v} \implies v\,\mathrm{d}v = \frac{\xi - 1}{r^2}\,\mathrm{d}r$$

The resulting expression is an equation of separate variables than can be integrated easily to define an integral of motion:

$$v^2 - \frac{2}{r}(1 - \xi) = K_1 \tag{6}$$

which introduces a control parameter in the generalization of the equation of the energy found by Roa and Peláez.[13] The constant of motion K_1 is solved from the initial conditions

$$K_1 = v_0^2 - \frac{2}{r_0}(1 - \xi) \tag{7}$$

If $\xi = 0$ the integral of motion (6) reduces to the equation of the Keplerian energy $\mathcal{E}_\mathrm{k}$, with

$$K_1(\xi = 0) \equiv 2\mathcal{E}_\mathrm{k} = v^2 - \frac{2}{r}$$

The values of the constant K_1 yield a natural classification of the resulting trajectories: *i)* ($K_1 < 0$, Elliptic spirals) The trajectory is bounded and never escapes to infinity. *ii)* ($K_1 = 0$, Parabolic spirals) They are equivalent to the logarithmic spirals. The particle reaches infinity with zero velocity

along a spiral branch. *iii)* ($K_1 > 0$, Hyperbolic spirals) The spiral exhibits an asymptote when approaching infinity, where the velocity is finite and nonzero. Type I spirals connect the origin with infinity. Type II spirals are symmetric, they have two asymptotes and there is a minimum radius that bounds the trajectory.

Dividing Eqs. (2) and (3) provides the relation

$$\frac{\mathrm{d}v}{v} = \frac{1-\xi}{1+\eta}\cot\psi\,(\mathrm{d}\psi + \mathrm{d}\theta)$$

By virtue of Eqs. (4–5) it follows an equation of separate variables

$$\frac{\mathrm{d}v}{v} + \frac{1-\xi}{1+\eta}\left(\cot\psi\,\mathrm{d}\psi + \frac{\mathrm{d}r}{r}\right) = 0$$

that can be integrated analytically and defines a first integral:

$$\ln v + \frac{1-\xi}{1+\eta}\left[\ln(\sin\psi) + \ln r\right] = \ln C \implies rv^{\gamma}\sin\psi = K_2 \tag{8}$$

where K_2 is a constant of motion to be solved from the initial conditions

$$K_2 = r_0 v_0^{\gamma}\sin\psi_0 \tag{9}$$

and $\gamma = (1+\eta)/(1-\xi)$. In the Keplerian case ($\xi = 0$ and $\eta = 0$) it is $\gamma = 1$, and the integral of motion (8) shows that

$$K_2 \equiv h_{\mathrm{k}} = rv\sin\psi$$

This means that K_2 reduces to the angular momentum of the Keplerian solution, h_{k}.

For $\gamma = 2$ (or $\eta = 1 - 2\xi$) the integral of motion (8) is the generalization of the conservation of the angular momentum discussed by Roa and Peláez.[14] In the following sections the original family of generalized logarithmic spirals is extended by introducing the control parameter ξ in the solution and assuming $\gamma = 2$, so $\eta = 1 - 2\xi$. Note that for $\gamma = 1$ it is $\eta = -\xi$. The equations of motion can be understood as Kepler's problem with a modified gravitational parameter.

The direction of the thrust vector

The tangent and normal vectors, $\mathbf{t}$ and $\mathbf{n}$, can be referred to the orbital frame $\mathcal{L} = \{\mathbf{i}, \mathbf{j}, \mathbf{k}\}$,

$$\mathbf{i} = \frac{\mathbf{r}}{r}, \qquad \mathbf{k} = \frac{\mathbf{h}}{h}, \qquad \mathbf{j} = \mathbf{k}\times\mathbf{i}$$

by means of $\mathbf{t} = \cos\psi\,\mathbf{i} + \sin\psi\,\mathbf{j}$ and $\mathbf{n} = -\sin\psi\,\mathbf{i} + \cos\psi\,\mathbf{j}$. The thrust acceleration from Eq. (1) becomes

$$\mathbf{a}_{\mathrm{p}} = \frac{1}{r^2}\left\{\left[\xi\cos^2\psi - (1-2\xi)\sin^2\psi\right]\mathbf{i} + (1-\xi)\sin\psi\cos\psi\,\mathbf{j}\right\}$$

The angle between the thrust direction and the radial direction, α, is defined by

$$\tan\alpha = \frac{(1-\xi)\sin 2\psi}{3\xi - 1 + (1-\xi)\cos 2\psi} \tag{10}$$

Roa and Peláez[14] noted that the original family of generalized logarithmic spirals ($\xi = 1/2$ and $\eta = 0$) requires an impulsive Δv for departing from circular orbits. This comes from the combination

of two factors: First, the velocity on the circular orbit is $v = 1/r$, what makes $K_1 = 0$ and the trajectory is a pure logarithmic spiral. In this case the flight-direction angle ψ is constant. Second, on a circular orbit it is always $\psi = \pi/2$ so the thrust vanishes. Since ψ remains constant along the logarithmic spiral the thrust acceleration will always be zero and the particle describes a Keplerian circular orbit. In the general case $\eta \neq 0$, the presence of a normal acceleration overcomes this limitation, and impulsive maneuvers are not required.

Symmetries

Two types of symmetries can be found in the original family of generalized logarithmic spirals.[13,14] First, the concept of $\mathscr{T}$-symmetry is an intrinsic property of the trajectory: if θ_m defines the direction of the axis of $\mathscr{T}$-symmetry then the trajectory satisfies $r(\theta_\mathrm{m} - \delta) = r(\theta_\mathrm{m} + \delta)$. Here δ denotes an arbitrary angular displacement. Second, the $\mathscr{C}$-symmetry refers to pairs of spirals. It arises from the fact that Eq. (9) relates to the departure flight-direction angle by means of its sine. This function is symmetric with respect to $\psi_0 = \pi/2$, meaning that there are two different values of ψ_0 that yield the same value of K_2. One trajectory is initially in raising regime, whereas its $\mathscr{C}$-symmetric is in lowering regime. Both trajectories share the same values of K_1 and K_2.

ELLIPTIC SPIRALS

Elliptic spirals relate naturally to Keplerian ellipses; the particle never escapes the potential well of the central body. When propagated forward and backwards in time the spiral falls towards the origin. The trajectory is $\mathscr{T}$-symmetric and the axis of $\mathscr{T}$-symmetry is equivalent to the apse line. There is a natural transition from raising regime to lowering regime at the apoapsis of the spiral. They are defined by negative values of the constant K_1. This determines the values of ξ that yield elliptic spirals, $\xi < 1 - r_0 v_0^2/2$.

From the integral of motion (8) and the condition $\sin\psi \leq 1$ it must be

$$\frac{K_2}{r v^\gamma} \leq 1 \implies r\left[K_1 + \frac{2}{r}(1-\xi)\right]^{\gamma/2} \geq K_2$$

Thanks to the assumption $\gamma = 2$ the previous expression simplifies to $K_1 r + 2(1-\xi) \geq K_2$ and shows that there is a maximum radius for the case of elliptic spirals ($K_1 < 0$):

$$r_\mathrm{max} = \frac{2(1-\xi) - K_2}{(-K_1)}$$

The condition on ξ that makes $K_1 < 0$ ensures $r_\mathrm{max} > 0$. The maximum radius can be seen as the apoapsis of the spiral. The velocity at r_max is

$$v_\mathrm{m} = \sqrt{\frac{K_2}{r_\mathrm{max}}} = \sqrt{\frac{-K_1 K_2}{2(1-\xi) - K_2}}$$

It is the minimum velocity that a particle can have on an elliptic spiral.

The flight-direction angle can be solved from the integral of motion (8) and results in

$$\sin\psi = \frac{K_2}{r v^\gamma} \equiv \frac{K_2}{r v^2} = \frac{K_2}{2(1-\xi) + K_1 r} \tag{11}$$

Only positive values of $\sin\psi$ will be considered. This restricts the solution to the case of prograde motions. Retrograde motions can be solved in an analogous way but are omitted for clarity. From Eq. (11) it follows

$$\cos\psi = \pm\frac{\sqrt{[2(1-\xi)+K_1 r]^2 - K_2^2}}{2(1-\xi)+K_1 r} \tag{12}$$

The choice of the sign depends on the regime of the spiral. If the spiral is in raising regime it is $\psi < \pi/2$ and therefore $\cos\psi > 0$. If the spiral is in lowering regime it is $\cos\psi < 0$. In what remains of the paper the first sign will always correspond to raising regime, and the second to lowering regime.

For $K_1 < 0$ Eq. (11) shows that K_2 is constrained to the open interval $0 < K_2 < 2(1-\xi)$. The tangent of ψ is obtained by combining Eqs. (11) and (12),

$$\tan\psi = \pm\frac{K_2}{\sqrt{[2(1-\xi)+K_1 r]^2 - K_2^2}}$$

and introducing this result in the quotient of Eqs. (5) and (4) it follows

$$\frac{\mathrm{d}\theta}{\mathrm{d}r} = \frac{\tan\psi}{r} \implies \mathrm{d}\theta = \pm\frac{K_2\,\mathrm{d}r}{r\sqrt{[2(1-\xi)+K_1 r]^2 - K_2^2}} \tag{13}$$

Integrating this equation determines the evolution of the polar angle θ as a function of the radial distance. This angle can be referred to the axis of symmetry, defined by $\theta(r_{\max}) = \theta_{\mathrm{m}}$, introducing the *spiral anomaly*:

$$\beta = \frac{\ell}{K_2}(\theta - \theta_{\mathrm{m}}) \tag{14}$$

The spiral anomaly evolves according to

$$\beta(\theta) = \mp\left|\operatorname{arccosh}\left\{\frac{r_{\max}}{r} - \frac{2(1-\xi)}{K_2}\left(1 - \frac{r_{\max}}{r}\right)\right\}\right| \tag{15}$$

having introduced the auxiliary parameter $\ell = \sqrt{4(1-\xi)^2 - K_2^2}$. The angle θ_{m} defines the orientation of the axis of symmetry, and can be solved directly from the initial conditions.

The equation for the trajectory $r = r(\theta)$ is solved in terms of the spiral anomaly by inverting Eq. (15),

$$\frac{r(\theta)}{r_{\max}} = \frac{2(1-\xi)+K_2}{2(1-\xi)+K_2\cosh\beta(\theta)} \tag{16}$$

The $\mathscr{T}$-symmetry of the trajectory is easily verified from this equation. This proves that introducing the control parameter ξ does not break the symmetries of the original family of solutions.

The time of flight

The time relates to the radial distance by means of the equation for the radial velocity, Eq. (4):

$$\frac{\mathrm{d}t}{\mathrm{d}r} = \frac{1}{v\cos\psi} = \pm\frac{\sqrt{r[2(1-\xi)+K_1 r]}}{\sqrt{\ell^2 + K_1 r[K_1 r + 4(1-\xi)]}} \tag{17}$$

This equation is integrated to provide the time of flight:

$$t(r) - t_{\mathrm{m}} = \pm\frac{rv}{K_1}\sqrt{\frac{1-\sin\psi}{1+\sin\psi}} \pm \frac{2[2(1-\xi)k'^2\Delta\Pi - K_2\Delta\mathrm{E}]\sqrt{1-\xi}}{(-K_1)^{3/2}\sqrt{K_2}}$$

that is referred to the time of passage through the apoapsis $r_{\max}$, denoted t_{m}. The solution is given in terms of the complete and the incomplete elliptic integrals of the second, $\mathrm{E}(\phi, k)$, and third kinds, $\Pi(p; \phi, k)$, namely $\Delta\mathrm{E} = \mathrm{E}(\phi, k) - \mathrm{E}(k)$ and $\Delta\Pi = \Pi(p; \phi, k) - \Pi(p; k)$. Their argument, modulus and parameter are, respectively:

$$\sin\phi = \frac{v_{\mathrm{m}}}{v}\sqrt{\frac{2}{1+\sin\psi}}, \qquad k = \sqrt{\frac{-K_1 r_{\max}}{4(1-\xi)}}, \qquad p = \frac{K_1 r_{\max}}{2K_2}$$

The complementary modulus k' is defined as $k' = \sqrt{1-k^2}$. The time of apoapsis passage is solved from the initial conditions through a direct particularization of the equation of the time of flight.

PARABOLIC SPIRALS

Parabolic spirals are equivalent to logarithmic spirals.[14] For arbitrary values of ξ the velocity is no longer the local circular velocity, but a generalization in terms of the control parameter:

$$v(r) = \sqrt{\frac{2(1-\xi)}{r}}$$

This equation shows how changing the value of the control parameter yields logarithmic spirals but with different velocity profiles. The value of the control parameter that makes the spiral logarithmic given a set of initial conditions is $\xi = 1 - r_0 v_0^2/2$.

Equation (11) governs the evolution of the flight-direction angle. Imposing $K_1 = 0$ in this equation yields $\sin\psi = K_2/[2(1-\xi)]$, so the flight-direction angle remains constant during the propagation. The differential equation connecting the polar angle θ with the radial distance is simply

$$\frac{\mathrm{d}\theta}{\mathrm{d}r} = \frac{\tan\psi}{r} = \pm\frac{K_2}{r\ell}$$

The equation of the trajectory takes the form

$$\frac{r(\theta)}{r_0} = \mathrm{e}^{\pm\ell(\theta-\theta_0)/K_2} \tag{18}$$

Observe that $\pm\ell/K_2 = \cot\psi$, which is constant, and therefore Eq. (18) is no other than the equation of a logarithmic spiral. The thrust acceleration in this case is not tangential to the trajectory, because the normal component defined in Eq. (1) is not zero in general. In fact, Eq. (10) shows that the thrust vector forms a constant angle with the radial direction.

As long as $K_1 = 0$ the trajectory will be a logarithmic spiral. If the flight-direction angle is fixed then changing the value of the control parameter ξ changes the magnitude of the velocity on the spiral, although the trajectory remains the same.

The time of flight

Imposing the condition $K_1 = 0$ in Eq. (17) results in a simple expression that can be integrated to provide the time of flight

$$t(r) - t_0 = \pm \frac{2\sqrt{2(1-\xi)}}{3\ell}\left(r^{3/2} - r_0^{3/2}\right)$$

This expression is referred directly to the initial conditions of the problem. The sign depends on the regime of the spiral like in the previous cases. It takes an infinite time to escape to infinity, meaning that parabolic spirals describe a spiral branch.

HYPERBOLIC SPIRALS

The family of hyperbolic generalized logarithmic spirals is defined by $K_1 > 0$. The integral of motion (6) sets no limits to the values that the radius can take. In fact, from this expression it follows that a particle traveling along a hyperbolic spiral reaches infinity with a finite, nonzero velocity $\lim_{r\to\infty} v^2 = K_1 \equiv C_3$. The constant K_1 is equivalent to the characteristic energy C_3 and readily provides the hyperbolic excess velocity. Once the initial conditions are fixed hyperbolic spirals appear for values of the control parameter satisfying $\xi > 1 - r_0 v_0^2/2$.

Equation (11) sets a dynamical constraint that relates the radius with K_1 and K_2, because $\sin\psi \leq 1$. When $K_1 > 0$ this expression holds even for $K_2 > 2(1-\xi)$, unlike for elliptic spirals, but the radius must then satisfy

$$r \geq \frac{K_2 - 2(1-\xi)}{K_1}$$

This equation defines the minimum radius that the spiral can reach. This behavior suggests that there are two different subfamilies of hyperbolic spirals, as it has already been anticipated. Hyperbolic spirals of Type I correspond to $K_2 < 2(1-\xi)$. The previous constraint on the radius holds naturally so they escape to infinity if they are in raising regime, and fall to the origin if in lowering regime. Hyperbolic spirals of Type II ($K_2 > 2(1-\xi)$) exhibit a minimum radius where the spiral transitions from lowering regime to raising regime. These spirals describe two asymptotes. The two types of spirals are separated by the limit case $K_2 = 2(1-\xi)$.

Hyperbolic spirals of Type I

This subfamily of spirals corresponds to $K_1 > 0$ and $K_2 < 2(1-\xi)$. The polar angle is solved by integrating Eq. (13) and becomes:

$$\theta(r) - \theta_0 = \pm \frac{K_2}{\ell} \ln\left\{\frac{r\sin\psi}{r_0\sin\psi_0}\left[\frac{2(1-\xi) - K_2\sin\psi_0 + \ell\,|\cos\psi_0|}{2(1-\xi) - K_2\sin\psi + \ell\,|\cos\psi|}\right]\right\}$$

The limit $r \to \infty$ determines the orientation of the asymptote:

$$\theta_{\text{as}} = \theta_0 \pm \frac{K_2}{\ell}\ln\left[\frac{K_2(\zeta - \ell - K_2\sin\psi_0 + \ell\,|\cos\psi_0|)}{r_0 K_1 \zeta \sin\psi_0}\right] \tag{19}$$

having considered the auxiliary variable $\zeta = 2(1-\xi) + \ell$.

This type of spiral is not $\mathscr{T}$-symmetric so the definition of the spiral anomaly given in Eq. (14) cannot be applied directly. Redefining the angular parameter $\beta(\theta)$ as

$$\beta(\theta) = \pm\frac{\ell}{K_2}(\theta_{\text{as}} - \theta)$$

the equation of the trajectory becomes

$$r(\theta) = \frac{\zeta \ell^2 / K_1}{\sinh\frac{\beta}{2}\left[4\zeta(1-\xi)\sinh\frac{\beta}{2} + (\zeta^2 - K_2^2)\cosh\frac{\beta}{2}\right]}$$

The sign of $\beta(\theta)$ depends on the regime of the spiral. So it does the value of the orientation of the asymptote given in Eq. (19). The regime of the spiral is easily determined from ψ_0. It is straightforward to verify the existence of an asymptote for $\theta = \theta_{\rm as}$ ($\beta = 0$).

The time of flight Inverting the equation of the radial velocity and integrating the resulting expression yields the time of flight,

$$t(r) = K_4 \pm \left\{ \frac{rv}{K_1}\sqrt{\frac{1+\sin\psi}{1-\sin\psi}} - \frac{2\left\{\mathrm{E} - (1-p)\Pi\right\}\sqrt{K_2(1-\xi)}}{K_1^{3/2}} \right\}$$

written in terms of a constant K_4. This constant can be easily solved from the previous equation particularized at the initial time. The solution is given in terms of the incomplete elliptic integrals of the second and third kinds, $\mathrm{E} = \mathrm{E}(\phi, k)$ and $\Pi = \Pi(p; \phi, k)$, being its arguments:

$$\sin\phi = \sqrt{\frac{K_1 r \sin\psi}{pK_2(1-\sin\psi)}}, \qquad k = \frac{1}{2}\sqrt{\frac{2(1-\xi)+K_2}{1-\xi}}, \qquad p = \frac{2(1-\xi)+K_2}{2K_2}$$

Hyperbolic spirals of Type II

For the case $K_1 > 0$ and $K_2 > 2(1-\xi)$ the condition $\sin\psi \leq 1$ provides

$$r_{\rm min} = \frac{K_2 - 2(1-\xi)}{K_1} \tag{20}$$

meaning that the spiral will never reach the origin. If the spiral is initially in lowering regime it will reach $r_{\rm min}$ and at this point it transitions to raising regime. In this case ℓ reads $\ell = \sqrt{K_2^2 - 4(1-\xi)^2}$.

The polar angle is solved from Eq. (13) and yields:

$$\theta(r) - \theta_{\rm m} = \pm\frac{K_2}{\ell}\left\{\frac{\pi}{2} + \arctan\left[\frac{2(1-\xi)[2(1-\xi)+K_1 r] - K_2^2}{\ell\sqrt{[2(1-\xi)+K_1 r]^2 - K_2^2}}\right]\right\} = \pm\frac{K_2}{\ell}\left\{\frac{\pi}{2} + \arctan\left[\frac{2(1-\xi) - K_2\sin\psi}{\ell\,|\cos\psi|}\right]\right\}$$

The angle $\theta_{\rm m}$ defines the direction of the axis of $\mathscr{T}$-symmetry. It can be solved from the initial conditions and the previous equation. Note that its definition depends on the regime of the spiral, because there are two possible $\mathscr{C}$-symmetric trajectories.

This equation can be inverted to provide the equation of the trajectory

$$\frac{r(\theta)}{r_{\rm min}} = \frac{2(1-\xi)+K_2}{2(1-\xi)+K_2\cos\beta} \tag{21}$$

having introduced the spiral anomaly:

$$\beta(\theta) = \frac{\ell}{K_2}(\theta - \theta_{\rm m})$$

Since the equation for the trajectory depends on the spiral anomaly by means of $\cos\beta$ the trajectory is $\mathscr{T}$-symmetric. The fact that there are two different values of β that cancel the denominator proves the existence of two distinct asymptotes. The asymptotes can be solved from the limit $r \to \infty$ in the equation for the polar angle and correspond to

$$\theta_{\mathrm{as}} = \theta_{\mathrm{m}} \pm \frac{K_2}{\ell}\left\{\frac{\pi}{2} + \arctan\left[\frac{2(1-\xi)}{\ell}\right]\right\}$$

The two asymptotes are given by the two different signs that appear in this equation. They are symmetric with respect to the apse line θ_{m}.

The time of flight The time of flight is obtained following the same technique applied to elliptic, parabolic and hyperbolic spirals of Type I. Integrating the inverse of the radial distance renders

$$t(r) - t_{\mathrm{m}} = \mp\left\{\frac{[K_2 + 2(1-\xi)]K_2\mathrm{E} - K_1 r_{\min}[K_2\mathrm{F} + 2(1-\xi)\Pi]}{K_1\sqrt{K_1K_2[K_2 + 2(1-\xi)]}} + \frac{2(1-\xi)}{K_1^{3/2}}\operatorname{arcsinh}\left[\frac{\sqrt{2K_1 r(rv^2 - K_2)}}{2\sqrt{K_2 rv^2 + (rv^2 - K_2)(1-\xi)}}\right] - \frac{v}{K_1^2}\sqrt{r^2v^4 - K_2^2}\right\}$$

The solution is given in terms of the incomplete elliptic integrals of the first, $\mathrm{F} \equiv \mathrm{F}(\phi, k)$, second, $\mathrm{E} \equiv \mathrm{E}(\phi, k)$, and third kinds, $\Pi \equiv \Pi(p; \phi, k)$. The arguments of the elliptic integrals are

$$\sin\phi = \frac{\sqrt{2(1-\xi)(1-\sin\psi)}}{k\sqrt{K_2 - 2(1-\xi)\sin\psi}}, \qquad k = \frac{2\sqrt{1-\xi}}{\sqrt{K_2 + 2(1-\xi)}}, \qquad p = \frac{2(1-\xi)}{K_2}$$

The time of flight is referred to t_{m}. It denotes the time of periapsis passage and is solved easily from the initial conditions.

ORBIT TRANSFERS

In this section the family of generalized logarithmic spirals is used for designing different transfer orbits. The control parameter provides a degree of freedom that can be adjusted at convenience to match certain requirements. In addition, the transfer can be decomposed in a number of arcs with different values of the control parameter, or even considering Keplerian arcs. The transition between two spiral arcs with different values of ξ is equivalent to changing the thrust magnitude and direction. No adjustments in the orbital velocity are required. The control parameter only affects the value of the constant K_1. By imposing $\gamma = 2$ the constant K_2 is made independent from the control parameter. Changing the value of ξ adjusts the values of the constant of the generalized energy, K_1, but not the values of K_2. If K_2 needs to be changed along the transfer a coast arc will be introduced.

Bitangent transfers

Consider the spiral transfer between two circular orbits of radii r_0 and $r_{\mathcal{F}}$. Along a spiral arc the evolution of the flight-direction angle ψ is monotonic, so if it is initially $\psi_0 = \pi/2$ (tangential departure) it is not possible to have $\psi_{\mathcal{F}} = \pi/2$ (tangential arrival) with one single spiral arc. Bitangent transfers are the composition of at least two continuous spiral arcs with different values of ξ. When $\psi = \pi/2$ the spiral is either a hyperbolic spiral at $r_{\min}$ or an elliptic spiral at $r_{\max}$. Parabolic spirals are not considered because of having a constant flight-direction angle.

The value of the constant K_2 corresponding to the first arc is $K_{2,1} = r_0 v_0^2 \sin\psi_0 = 1$. Since the control parameter does not affect the value of K_2 both spiral arcs share the same values of $K_2 \equiv K_{2,1} = K_{2,2} = 1$. The constant of the generalized energy on the first spiral arc takes the form

$$K_{1,1} = v_0^2 - \frac{2(1-\xi_1)}{r_0} = \frac{2\xi_1 - 1}{r_0}$$

For transfers with $r_0 < r_{\mathcal{F}}$ the first arc is a hyperbolic spiral of Type II (with $r_0 = r_{\min}$) and the second arc is an elliptic spiral (with $r_{\max} = r_{\mathcal{F}}$). The condition $r_0 = r_{\min}$ is satisfied naturally when imposing $K_2 = 1$. The radial distance at the transition point $\mathcal{A}$ is solved from the equation of the trajectory, Eq. (21):

$$\frac{r_{\mathcal{A}}}{r_0} = \frac{3 - 2\xi_1}{2(1-\xi_1) + \cos \ell_1 \theta_{\mathcal{A}}} \tag{22}$$

Similarly, the arrival spiral arc is defined by

$$K_{1,2} = v_{\mathcal{F}}^2 - \frac{2(1-\xi_2)}{r_{\mathcal{F}}} = \frac{2\xi_2 - 1}{r_{\mathcal{F}}}$$

and $K_{2,2} = 1$. From this equation it immediately follows that $r_{\max} = r_{\mathcal{F}}$. The conditions at the transition point are obtained from the equation of the trajectory Eq. (16):

$$\frac{r_{\mathcal{A}}}{r_{\mathcal{F}}} = \frac{3 - 2\xi_2}{2(1-\xi_2) + \cosh\{\ell_2[\theta_{\mathcal{A}} - (2n+1)\pi]\}} \tag{23}$$

The maximum radius occurs at $\theta_{\mathrm{m}} = (2n+1)\pi$, where n is the number of revolutions. Dividing Eqs. (22) and (23) provides a relation between ξ_1 and ξ_2,

$$\frac{r_{\mathcal{F}}}{r_0} = \frac{3 - 2\xi_1}{3 - 2\xi_2} \left\{ \frac{2(1-\xi_2) + \cosh\{\ell_2[\theta_{\mathcal{A}} - (2n+1)\pi]\}}{2(1-\xi_1) + \cos \ell_1 \theta_{\mathcal{A}}} \right\} \tag{24}$$

Due to the conservation of K_1 the values of $K_{1,2}$ at $\mathcal{F}$ and $\mathcal{A}$ are the same. The velocity-matching condition follows from the integral of the generalized energy,

$$\frac{2\xi_2 - 1}{r_{\mathcal{F}}} = \frac{2\xi_1 - 1}{r_0} + \frac{2(\xi_2 - \xi_1)}{r_{\mathcal{A}}}$$

This condition yields an expression of ξ_2 as a function of ξ_1 and the boundary conditions,

$$\xi_2 = \frac{[(1-2\xi_1)r_{\mathcal{F}} - r_0]r_{\mathcal{A}} + 2\xi_1 r_0 r_{\mathcal{F}}}{2r_0(r_{\mathcal{F}} - r_{\mathcal{A}})} \tag{25}$$

The problem of designing a bitangent transfer then reduces to solving for ξ_1 in Eq. (24). The value of the control parameter on the second arc, ξ_2, is given by Eq. (25). There is one degree of freedom in the solution. Under this formulation it corresponds to the angular position of the node defining the transition point, $\theta_{\mathcal{A}}$. In addition, the number of revolutions can be adjusted by changing the values of n.

In a similar fashion, when $r_0 > r_{\mathcal{F}}$ the equation to be solved for ξ_1 transforms into

$$\frac{r_{\mathcal{F}}}{r_0} = \frac{3 - 2\xi_1}{3 - 2\xi_2} \left\{ \frac{2(1-\xi_2) + \cos\{\ell_2[\theta_{\mathcal{A}} - (2n+1)\pi]\}}{2(1-\xi_1) + \cosh \ell_1 \theta_{\mathcal{A}}} \right\} \tag{26}$$

Recall that $\ell_i = \sqrt{|1 - 4(1-\xi_i)^2|}$. Equation (25) still holds in this case.

Figure 2 shows two examples of bitangent transfers with 0 and 1 revolutions. The problem is based on an Earth to Mars transfer, where $r_{\mathcal{F}}/r_0 = 1.527$. The transition point is selected arbitrarily. The departure spiral arc corresponds to a hyperbolic spiral of Type II in raising regime, whereas the second arc corresponds to an elliptic spiral in lowering regime. Their minimum and maximum radii are r_0 and $r_{\mathcal{F}}$, respectively.

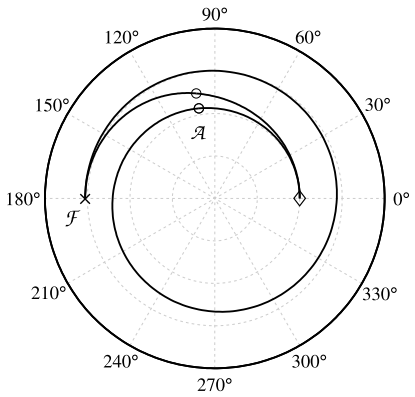

Figure 2: **Bitangent transfers with ∘ marking the transition point**

Low-thrust transfers are considered because they typically allow increasing the mass delivered to the final orbit. Figure 3 compares the fraction of mass that can be inserted into the final orbit using the Hohmann and the spiral transfers. The values of the specific impulse for the electric propulsion system and for the impulsive maneuvers are 2500 s and 250 s, respectively. In this example the 0-revolutions spiral transfer allows to deliver over 50% of the initial mass, and the 1-revolution case increases this percentage up to 75%. For the case of the Hohmann transfer the fraction of delivered mass falls to roughly 10% of the initial mass.

The time of flight for the different types of transfers is plotted in Fig. 4. The 0-revolutions spiral transfer is geometrically equivalent to the Hohmann transfer and the time of flights are comparable. Depending on the transition point spiral transfers that are either slower or faster than the Hohmann transfer can be found. Increasing the number of revolutions can reduce the propellant consumption, but the time of flight grows significantly. In this example the bitangent spiral transfer with one revolution increases the time of flight by a factor of three when compared with the Hohmann transfer, and for two revolutions the time of flight increases approximately by a factor six.

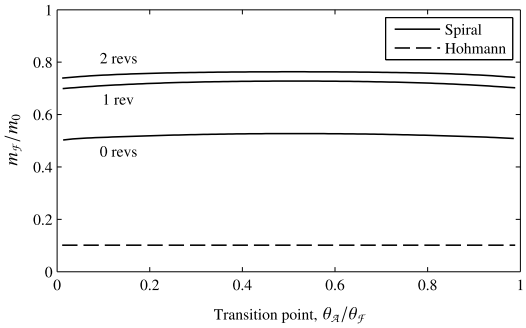

Figure 3: **Fraction of mass delivered to the final circular orbit**

Figure 3 suggests that there is a particular position of the transition point $\theta_{\mathcal{A}}$ that maximizes the mass delivered into orbit. The 0-revolutions case is geometrically equivalent to the Hohmann transfer and can be compared directly in terms of mass delivered into orbit and time of flight. When considering the optimal transition point the spiral transfer delivers into Martian orbit 52.74% of the launch mass, whereas the Hohmann transfer can only deliver 10.12%. The time of flight for the Hohmann transfer is 259.38 d. The spiral transfer turns out to be faster, reducing the time of flight to 257.05 d.

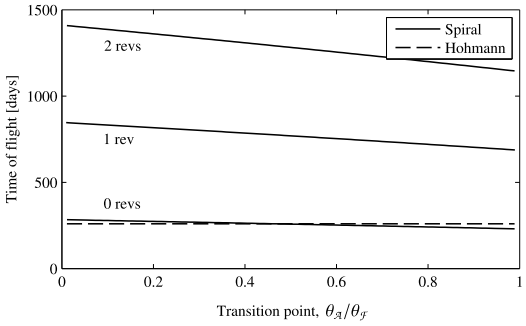

Figure 4: **Time of flight for Earth to Mars bitangent transfers**

The optimum spiral transfer is found by adequately selecting the transition point $\theta_{\mathcal{A}}$. Under the assumption that the specific impulse I_{sp} remains constant the mass fraction is given by Tsiolkovsy's

equation, where the Δv due to thrust is the time integral

$$\Delta v_{\rm thr} = \int_{t_0}^{t_{\mathcal{A}}} a_{\rm p1}\,{\rm d}t + \int_{t_{\mathcal{A}}}^{t_{\mathcal{F}}} a_{\rm p2}\,{\rm d}t$$

The integral of the thrust acceleration is decomposed in two arcs: the acceleration along the departure arc, $a_{\rm p1}$, is defined by ξ_1, while the acceleration along the second arc, $a_{\rm p2}$, is defined by ξ_2. The change in the thrust profile at $\theta_{\mathcal{A}}$ is the correction that the initial arc requires in order to meet the the boundary conditions at arrival. Hence, the optimal solution is the one that the requires the smallest correction, i.e. the transfer on which the difference $|a_{\rm p1} - a_{\rm p2}|$ at the transition point is minimum. The optimum transition point for maximizing the mass delivered into orbit is the one that minimizes the function $f_{\rm b}(\theta_{\mathcal{A}}) = |a_{\rm p1} - a_{\rm p2}|$.

Transfers between arbitrary state vectors. Introducing coast arcs

The integral of motion (6) readily shows that changing the control parameter ξ only adjusts the value of K_1. The first integral (8) is not affected by the control parameter when the value of γ is fixed. If the values of K_1 on the departure and arrival spiral arcs are the same no further corrections are required. However, in a general case $K_{2,1} \neq K_{2,2}$ and therefore the constant K_2 needs to be adjusted. A coast arc is introduced in order to connect the departure and arrival spiral arcs with the adequate values of K_2. The first spiral arc links the departure point with a node $\mathcal{A}$. A Keplerian orbit connects $\mathcal{A}$ and $\mathcal{B}$, and the final thrust leg connects $\mathcal{B}$ and the final point, $\mathcal{F}$. If the difference between $K_{2,1}$ and $K_{2,2}$ is small the coast arc will be short.

The transfer from an initial position and velocity vectors, $\mathbf{r}_0$ and $\mathbf{v}_0$, to a given state $\mathbf{r}_{\mathcal{F}}$ and $\mathbf{v}_{\mathcal{F}}$ imposes three constraints on the solution at $\theta_{\mathcal{F}}$. These are $r = r_{\mathcal{F}}$, $v = v_{\mathcal{F}}$ and $\psi = \psi_{\mathcal{F}}$. The control parameters on both spiral arcs ξ_1 and ξ_2 can be adjusted to solve the transfer, together with the orientation of the nodes $\mathcal{A}$ and $\mathcal{B}$, defined by $\theta_{\mathcal{A}}$ and $\theta_{\mathcal{B}}$. Having four variables for only three constraints there is a degree of freedom in the solution. The preferred choice is to use the position of the first node $\mathcal{A}$ as the free parameter and then solve for ξ_1, ξ_2 and the position of node $\mathcal{B}$.

The initial conditions define the value of the constants K_1 and K_2 on the first spiral arc:

$$K_{1,1} = v_0^2 - \frac{2(1-\xi_1)}{r_0} \qquad \text{and} \qquad K_{2,1} = r_0 v_0^2 \sin\psi_0$$

just like the arrival conditions define $K_{1,2}$ and $K_{2,2}$ by replacing 0 by $\mathcal{F}$ and 1 by 2 in the previous. The first arc can be propagated to $\mathcal{A}$ using the corresponding equation for the trajectory. The conditions at $\mathcal{A}$ provide the eccentricity, semimajor axis and argument of periapsis of the Keplerian orbit:[14]

$$e = \sqrt{K_{2,1}^2 + 1 - 2K_{2,1}\sin\psi_{\mathcal{A}}} \tag{27}$$

$$a = \frac{r_{\mathcal{A}}}{2\xi_1 - K_{1,1} r_{\mathcal{A}}} \tag{28}$$

$$\omega = \text{atan2}(-\sin\theta_{\mathcal{A}} - K_{2,1}\cos(\theta_{\mathcal{A}} + \psi_{\mathcal{A}}), K_{2,1}\cos(\theta_{\mathcal{A}} + \psi_{\mathcal{A}}) - \sin\theta_{\mathcal{A}}) \tag{29}$$

The values of K_1 that a spiral will take if the thrust is switched on again at some point of the Keplerian orbit are $K_1 = (2a\xi - r)/(ra)$. The velocity-matching condition at $\mathcal{B}$ then yields

$$\frac{2a\xi_2 - r_{\mathcal{B}}}{r_{\mathcal{B}} a} = v_{\mathcal{F}}^2 - \frac{2(1-\xi_2)}{r_{\mathcal{F}}}$$

Recall that the semimajor axis and eccentricity have already been solved from the conditions at $\mathcal{A}$. The state at node $\mathcal{B}$ is solved analytically from Kepler's problem. The remaining two constraints are set on the values of the radius and flight-direction angle at $\mathcal{F}$. In sum, the variables $\{\xi_1, \xi_2, \theta_\mathcal{B}\}$ are solved from the system of nonlinear equations:

$$\begin{cases} \dfrac{2a\xi_2 - r_\mathcal{B}}{r_\mathcal{B} a} + \dfrac{2(1-\xi_2)}{r_\mathcal{F}} - v_\mathcal{F}^2 = 0 \\ r_\mathcal{F} - r(\theta_\mathcal{F}; K_{1,2}, K_{2,2}, r_\mathcal{B}, \theta_\mathcal{B}, \xi_2) = 0 \\ \psi_\mathcal{F} - \psi(\theta_\mathcal{F}; K_{1,2}, K_{2,2}, r_\mathcal{B}, \theta_\mathcal{B}, \xi_2) = 0 \end{cases} \tag{30}$$

The conditions at $\mathcal{B}$ have already been obtained by propagating the Keplerian arc.

Similarly, the evolution of K_2 on the coast leg renders

$$K_2 = \sqrt{1 + 2e\cos\nu + e^2} \tag{31}$$

where ν denotes the true anomaly. In Fig. 5 it is possible to study the evolution of the values of K_2 and the flight-direction angle depending on the position inside a Keplerian orbit. Spirals arriving/departing in raising regime correspond to points in the Keplerian orbit that are between periapsis and apoasis, whereas spirals in lowering regime arrive to/depart from points between apoapsis and periapsis.

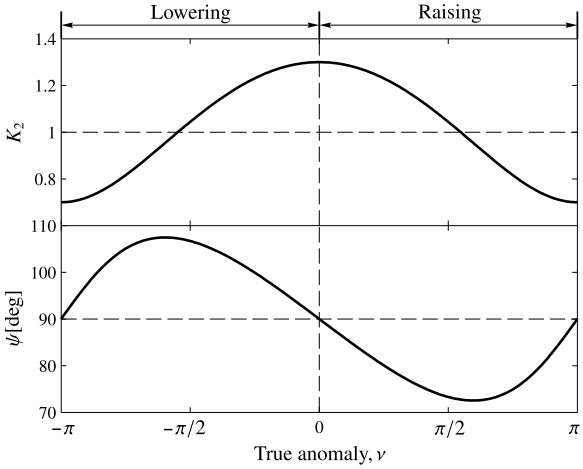

Figure 5: Evolution of K_2 and ψ on a Keplerian orbit ($e = 0.3$).

At $\mathcal{B}$ the true anomaly is simply $\nu_\mathcal{B} = \theta_\mathcal{B} - \omega$. The position of the node $\mathcal{B}$ can be solved from the compatibility equation on K_2, which yields the relation

$$\cos\nu_\mathcal{B} = \frac{K_{2,2}^2 - (1+e^2)}{2e} \tag{32}$$

There are two possible solutions to this equation depending on which quadrant the solution is in. As shown in Fig. 5 if $\nu_\mathcal{B} \in (0, \pi)$ the second spiral arc will be in raising regime at $\mathcal{B}$. If $\nu_\mathcal{B}$ then the second spiral departs in lowering regime. If $r_\mathcal{B} < r_\mathcal{F}$ then $\nu_\mathcal{B} \in (0, \pi)$, and if $r_\mathcal{B} > r_\mathcal{F}$ then $\nu_\mathcal{B} \in (\pi, 2\pi)$. This criterion is valid for direct transfers from $\mathcal{B}$ to $\mathcal{F}$. In most practical applications the spirals are direct. If the spiral transfer is indirect then the previous criterion is inverted.

The velocity-matching condition provides the relation

$$\xi_2 = \frac{[2a - r_\mathcal{F}(1 + a v_\mathcal{F}^2)] r_\mathcal{B}}{2a(r_\mathcal{B} - r_\mathcal{F})} \tag{33}$$

Thanks to the previous expressions the system of equations defined in Eq. (30) reduces to one single transcendental equation,

$$r_\mathcal{F} - r(\theta_\mathcal{F}; K_{12}, K_{22}, r_\mathcal{B}, \theta_\mathcal{B}, \xi_2) = 0 \tag{34}$$

to be solved for ξ_1. On every iteration the values of $\{\xi_2, \theta_\mathcal{B}\}$ are solved from Eqs. (33) and (32), respectively. Recall that $\theta_\mathcal{B} = \omega + \nu_\mathcal{B}$.

Figure 6 shows two examples of generic spiral transfers including a coast arc. The first example is the result of circularizing an elliptic orbit considering 0-revolutions spiral arcs. The switch point $\mathcal{A}$ can be adjusted at convenience. Two different solutions to the same transfer problem are presented in the first example. The second example corresponds to an Earth to Ceres transfer. In this case the correction required on K_2 is small and therefore the coast arc is almost negligible. Different solutions are displayed corresponding to different positions of the transition point $\mathcal{A}$. In this example the coast arc is so small that it cannot be distinguished.

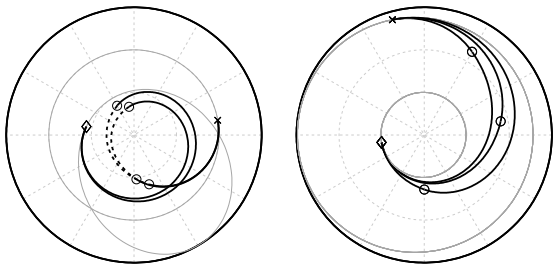

(a) Circularization (b) Earth to Ceres

Figure 6: Examples of transfers between arbitrary orbits with short coast arcs. The departure point is $\diamond$, the points $\mathcal{A}$ and $\mathcal{B}$ are denoted by $\circ$, and the arrival point is $\times$. The coast arcs are plotted using dashed lines.

GENERIC PERIODIC ORBITS

Relying on the symmetry properties of the generalized logarithmic spirals arbitrary periodic orbits can be generated. Numerically the problem reduces to solving a bitangent spiral transfer where the orientation of the arrival point is adjusted depending on the periodicity conditions. Periodic orbits are constructed by combining elliptic and Type II hyperbolic spiral arcs; the exterior radius of the orbit corresponds to $r_{\max}$, whereas the interior radius defines $r_{\min}$. Only two arcs are required to build a periodic orbit; they are repeated sequentially according to the symmetries of the spirals.

Consider a periodic orbit with $s = 3, 4, 5, \ldots$ lobes. If the spiral departs from the maximum radius ($\theta = 0$) then the minimum radius will be reached at $\theta = \pi\Lambda(s)$. The parameter $\Lambda(s)$ depends on the number of lobes and determines the configuration of the periodic orbit. Typical values of $\Lambda(s)$ are $\Lambda(s) = (s - j)/s$, with $j = 1, 2, \ldots, s - 1$. Given a transition point $\theta_{\mathcal{A}}$ the method derived for solving coaxial bitangent transfers can be extended to compute the values of ξ_1 and ξ_2 defining a generic periodic orbit. When the periodic orbit intersects itself at least once it is called an interior periodic orbit ($j < s - 1$), and exterior otherwise ($j = s - 1$). Figure 7 depicts the construction of an interior periodic orbit with $s = 3$ and $\Lambda = (s - 1)/s = 2/3$.

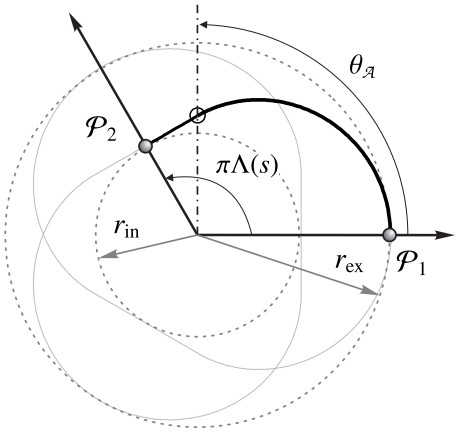

Figure 7: **Construction of an interior periodic orbit with** $s = 3$

The symmetry properties of the spirals guarantee that if the second spiral arc reaches a minimum $r_{\min} = r_{\text{in}}$ at $\theta_{\text{m}} = (s - 1)\pi/s$ then the resulting trajectory is a periodic orbit with s lobes. For $r_0 = r_{\text{in}}$ or $r_0 = r_{\text{ex}}$ the equation to be solved for ξ_1 is, respectively,

$$\frac{r_{\text{ex}}}{r_{\text{in}}} = \frac{3 - 2\xi_1}{3 - 2\xi_2}\left\{\frac{2(1 - \xi_2) + \cosh[\ell_2(\theta_{\mathcal{A}} - \Lambda\pi)]}{2(1 - \xi_1) + \cos \ell_1\theta_{\mathcal{A}}}\right\}, \quad \frac{r_{\text{in}}}{r_{\text{ex}}} = \frac{3 - 2\xi_1}{3 - 2\xi_2}\left\{\frac{2(1 - \xi_2) + \cos[\ell_2(\theta_{\mathcal{A}} - \Lambda\pi)]}{2(1 - \xi_1) + \cosh \ell_1\theta_{\mathcal{A}}}\right\}$$

Figure 8 displays a number of example interior and exterior periodic orbits generated by combining two spiral arcs. The entire orbit is generated by symmetrically extending a bitangent transfer defined by two arcs.

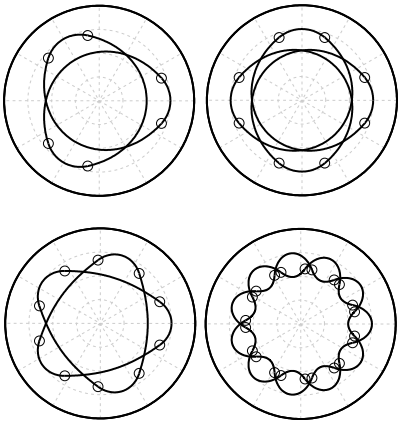

Figure 8: **Examples of periodic orbits**

THE MAXIMUM THRUST ACCELERATION

The family of generalized logarithmic spirals originates from a shape-based method, but it is actually the solution to the dynamics defined by the thrust acceleration profile from Eq. (1). This section is devoted to analyzing the details of the this acceleration. In particular, we study the maximum acceleration reached along the transfer so transfers that violate the limitations on the maximum thrust can be rejected.

The magnitude of the thrust acceleration is

$$a_{\mathrm{p}} = \frac{1}{r^2}\sqrt{\xi^2\cos^2\psi + (1-2\xi)^2\sin^2\psi} \tag{35}$$

Unbounded spirals (parabolic or hyperbolic) in raising regime escape to infinity. The acceleration when approaching infinity abides by $\lim_{r\to\infty} a_{\mathrm{p}} = 0$. For the case of parabolic spirals ($K_1 = 0$) the angle ψ is known to be constant so that a_{p} is governed exclusively by the power law $1/r^2$. The maximum and minimum acceleration corresponds to the minimum and maximum radius, respectively.

The magnitude of the thrust evolves according to the law $1/r^2$ and to $\cos^2\psi$. But if the control parameter is $\xi = 1$ or $\xi = 1/3$ the dependency with the flight-direction angle disappears ($\xi = 1$ is rejected because it has been considered to be $\xi < 1$). For $\xi = 1/3$ it is simply $a_{\mathrm{p}} = 1/(3r^2)$. Like in the case of parabolic spirals the maximum acceleration occurs at the minimum radius.

The maximum acceleration for elliptic and parabolic spirals corresponds to the minimum radius reached on the spiral. For hyperbolic spirals of Type I when the radius increases the value of $\cos\psi$ decreases, so the minimum acceleration corresponds simply to the maximum radius. Similarly, the maximum acceleration corresponds to the minimum radius. When the spiral is hyperbolic and of Type II the angle ψ decreases and transitions from lowering to raising regime occur. The evolution of $\cos^2\psi$ can compensate the power law $1/r^2$ and additional extrema might appear. At periapsis ($\psi = \pi/2$) the acceleration reduces to

$$a_{\mathrm{p,per}} = \frac{|1-2\xi|}{r_{\mathrm{min}}^2} \tag{36}$$

Roa *et al.*[14] already noted that in the case $\xi = 1/2$ the acceleration vanishes at periapsis, being the minimum acceleration reached on the spiral. Provided that $\lim_{r\to\infty} a_{\mathrm{p}} = 0$ the acceleration reaches a maximum value between r_{min} and $r \to \infty$. Let Q denote this point. From the derivative of Eq. (35) with respect to r having introduced Eq. (12) it follows that the maximum acceleration is reached at

$$r_Q = \frac{6K_1K_2(1-\xi)}{R^{1/3}}\left[(1-3\xi)K_2\cos\left(\frac{\vartheta+2\pi}{3}\right) - \xi\sqrt{2(1-\xi)(3\xi-1)}\right]$$

where

$$R = 54K_1^6K_2^3\xi^3\sqrt{2(3\xi-1)^3(1-\xi)^3}, \qquad \vartheta = \arctan\left[\frac{\sqrt{2[K_2^2(3\xi-1)-2\xi^2(1-\xi)]}}{2\xi\sqrt{1-\xi}}\right]$$

As the control parameter separates from $\xi = 1/2$ the magnitude of the acceleration at periapsis increases. There is an upper and a lower limit for which the acceleration at periapsis equals the magnitude of the acceleration at r_Q, ξ^+ and ξ^- respectively. If the control parameter is over/below the upper/lower limit then $a_{\mathrm{p,per}}$ becomes the maximum acceleration reached on the spiral. These limits are the solutions to the transcendental equation

$$a_{\mathrm{p,per}} - \frac{1}{{r_Q}^2}\sqrt{(1-2\xi)^2 + (3\xi-1)(1-\xi)\cos^2\psi_Q} = 0 \tag{37}$$

The constant K_1 relates to the initial conditions and the control parameter by means of Eq. (7), whereas K_2 is completely determined by the initial conditions. In this equation $\psi_Q = \psi(r_Q)$. If $\xi \in [\xi^-, \xi^+]$ then the maximum acceleration on a hyperbolic spiral of Type II occurs at r_Q. Conversely, if $\xi \notin [\xi^-, \xi^+]$ the maximum acceleration occurs at periapsis and it is defined by Eq. (36).

The results presented in this section are summarized as follows: the problem of finding the maximum acceleration in a spiral transfer from r_0 to $r_\mathcal{F}$ reduces to finding the radius r^* that maximizes Eq. (36). For elliptic, parabolic and hyperbolic spirals of Type I spirals it is simply $r^* = \min(r_0, r_\mathcal{F})$. For hyperbolic spirals of Type II one first has to solve Eq. (37) in order to obtain the limits ξ^- and ξ^+ between which $a_{\mathrm{p,per}} < a_{\mathrm{p}}(r_Q)$. Then, the values that r^* take are

$$\xi \in [\xi^-, \xi^+] : \begin{cases} \min(r_0, r_\mathcal{F}), & r_Q \le \min(r_0, r_\mathcal{F}),\ \mathrm{D} \\ \max(r_0, r_\mathcal{F}), & r_Q \ge \max(r_0, r_\mathcal{F}),\ \mathrm{D}\ ; \\ r_Q, & \text{rest} \end{cases} \qquad \xi \notin [\xi^-, \xi^+] : \begin{cases} r_{\min}, & \mathrm{I} \\ \min(r_0, r_\mathcal{F}), & \text{rest} \end{cases}$$

Here D and I denote direct and indirect transfers, respectively. The maximum acceleration is solved by substituting $r = r^*$ in Eq. (35).

MULTINODE TRANSFERS

We have shown that transfers between circular orbits require at least one transition node, whereas transfers between arbitrary state vectors require a coast arc. An arbitrary number of nodes can be introduced in order to increase the flexibility of the solution.

Consider the problem of finding transfers between circular orbits introducing $N \ge 1$ nodes. Let θ_n denote the orientation of the n-th node. There are $2N-1$ degrees of freedom in the solution: the position of the nodes $(\theta_1, \theta_2, \theta_3, \ldots, \theta_N)$ and the control parameters of the interior arcs $(\xi_2, \xi_3, \ldots, \xi_{N-1})$. The arc connecting nodes $n-1$ and n is labeled the n-th arc. With this, the initial arc connecting θ_0 and θ_1 is labeled "1". The final arc, connecting θ_N and $\theta_\mathcal{F}$, is denoted by $\mathcal{F}$. The problem consists in solving for ξ_1 given the position of the nodes and the values of the control parameter for the intermediate arcs.

The trajectory is propagated sequentially through the nodes $r_n = r(\theta_n; \xi_n)$, with $n = 1, 2, \ldots, N$ and considering the initial conditions $(r_{n-1}, v_{n-1}, \theta_{n-1}, \psi_{n-1})$ defined by the previous node. The final arc needs to satisfy two conditions: first, the velocity-matching condition

$$v_N^2 = K_{1,\mathcal{F}} + \frac{2(1-\xi_\mathcal{F})}{r_N} \implies \xi_\mathcal{F} = \frac{2r_\mathcal{F} - r_N[2 + r_\mathcal{F}(v_N^2 - v_\mathcal{F}^2)]}{2(r_\mathcal{F} - r_N)}$$

Second, the boundary condition $r_{\mathcal{F}} = r(\theta_{\mathcal{F}}; \xi_{\mathcal{F}})$. Figure 9 shows two examples of multinode transfers between two circular orbits. Each figure presents two spiral transfers that depart/arrive from/to the same exact state vectors. The differences between the transfers are the positions of the nodes and the values of the control parameters. It is worth to emphasize that the transitions at the nodes are continuous (no additional Δv's are required) and no correcting maneuvers are required at departure nor arrival.

Introducing multiple nodes in transfers between arbitrary state vectors is a simple procedure: the problem reduces to solving a thrust-coast-thrust transfer, but the boundary conditions are given by the forward/backwards propagation of the additional spiral arcs. Consider that there are N_1 spiral arcs until the thrust is switched off, and N_2 arcs between the point where the thrust is switched on again and the arrival point. The initial conditions to be considered for solving Eq. (34) are defined by the final state after propagating the spirals $1, 2, \ldots, N_1 - 1$. The arrival conditions are obtained from the backwards propagation of the $N_2, N_2 - 1, \ldots, 2$ arcs in the second leg.

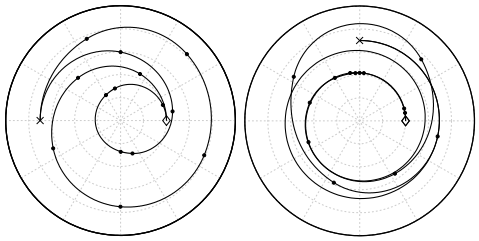

(a) 1 revolution (b) 2 revolutions

Figure 9: Examples of bitangent transfers with $N = 7$. The nodes are $\bullet$, $\diamond$ is the departure point and $\times$ is the arrival point.

LOW-THRUST GRAVITY-ASSIST TRANSFER

In this section we design a mission launched from the Earth to rendezvous with Ceres after a flyby about Mars. The mission has been analyzed in a number of publications.[15,3] We prove that the controlled generalized logarithmic spirals (CGLS) can indeed reproduce preliminary solutions that are known to be close to the optimized trajectory. The orbits are assumed to be contained in the ecliptic plane, as defined in Table 1.

Table 1: **Reference (coplanar) orbits**

	Units	Earth	Mars	Ceres
a	AU	1.0000	1.5237	2.7656
e	–	0.0162	0.0936	0.0794
$\omega + \Omega$	deg	103.93	336.06	154.60

Table 2: **Spiral segments**

	Type	ξ	K_1	K_2
EM-1	H-II	0.4936	0.0885	1.1021
EM-2	H-II	0.5181	0.0111	0.9684
MC-1	H-II	0.4983	0.0912	1.1371
MC-2	Ellip	0.4938	-0.0279	0.9291

The specific impulse is assumed to be constant and equal to 3000 s. The spacecraft departs from the Earth on May 6, 2003 with $v_\infty = 1.6$ km/s at launch. The mass injected into orbit is 568 kg. Transfer legs include an intermediate coast arc. In the EM leg both spirals are hyperbolic of Type II (H-II). The spiral arcs are described in Table 2. In the Mars-Ceres (MC) leg the first spiral is also hyperbolic of Type II, whereas the second spiral is elliptic. The performance of the CGLS is compared with the solutions provided by Petropoulos and Longuski[3] and Sauer[15] in Table 3. The MC leg is solved in order to rendezvous with Ceres. The times of flight are[3] 271 and 862 days for the EM and MC transfer legs, respectively. The solution found with the CGLS yields the same propellant mass fraction as STOUR-LTGA, but requires no additional impulsive Δv for the final rendezvous with Ceres. Given the relatively low specific impulses of liquid propellants this final maneuver may increase significantly the propellant mass fraction. Note that Sauer used a more sophisticated model for the thruster, and he selected June 8, 2003, for the launch date.

Table 3: **Comparison of the CGLS solution with STOUR-LTGA, GALLOP and Sauer's solution**

	Units	CGLS	STOUR-LTGA[3]	GALLOP[3]	Sauer[15]
Launch v_∞	km/s	1.600	1.600	1.600	1.600
Mars flyby v_∞	km/s	1.590	1.435	1.920	–
Flyby altitude	km	562	5432	200	–
Propellant mass fraction	–	0.256	0.256	0.234	0.275
Arrival v_∞	km/s	0.000	0.237	0.000	0.000
TOF Earth-Mars	days	271	271	271	250
TOF Mars-Ceres	days	862	862	862 (739)	845
TOF total	days	1133	1133	1133 (1010)	1095

The trajectory is plotted in Fig. 10. Both the EM and the MC legs include coast arcs to gain control over the final state. Right after launch there is a short thrust arc in order to increase the energy of the intermediate Keplerian orbit. The thrust is switched on again when the values of K_1 and K_2 are compatible with a feasible flyby about Mars. The flyby is designed so it yields adequate values of the constants of motion. The MC leg is solved from Eq. (34) having selected the switch point that minimizes the propellant mass fraction.

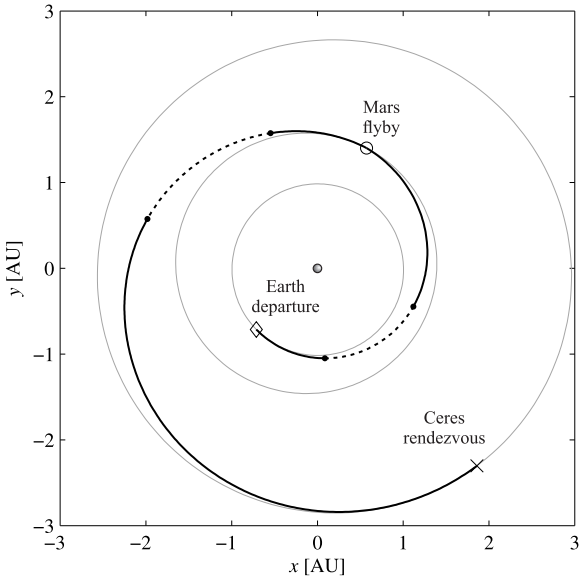

Figure 10: Earth-Mars-Ceres transfer. Dashed lines are coast arcs.

The magnitude of the thrust required for the mission is plotted in Fig. 11. It is worth noticing that the required thrust exhibits some peaks that exceed the limit thrust adopted by Petropoulos and Longuski;[3] they considered that the available thrust is 95 mN at 1 AU and it decreases with the power law $1/r^2$. However, due to the coast arcs the final result is a propellant mass fraction that is comparable to the optimized solution, as shown in Table 3.

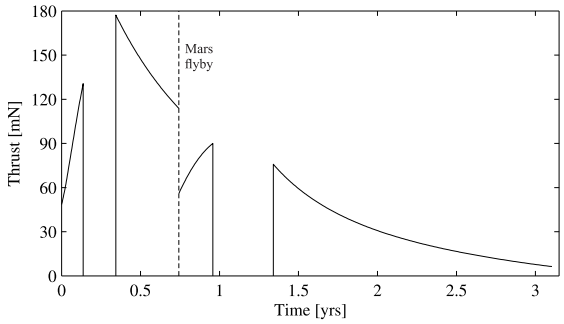

Figure 11: **Thrust magnitude**

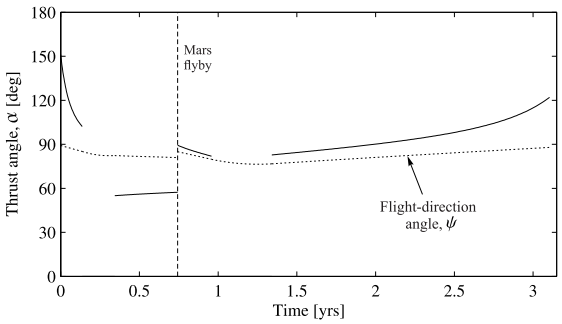

Figure 12: **Thrust angle**

The orientation of the thrust depends on the values of the control parameters (see Table 2) and on the evolution of the flight-direction angle. Figure 12 shows how the thrust angle evolves compared to the flight-direction angle. The orientation (and magnitude) of the thrust vector is adjusted in order

to meet the constraints on the time of flight. In addition, in the MC leg the values of the control parameter are defined so that the final velocity matches that of Ceres. Along the final spiral arc the magnitude of the thrust decreases and the thrust angle separates from the flight-direction angle for matching the velocities.

CONCLUSIONS

The main limitation of the original family of generalized logarithmic spirals, which is the fact that the solution is unique given a set of initial conditions, is overcome by introducing a control parameter in the thrust vector. This additional degree of freedom defines a family of solutions for any given set of initial conditions. The improved flexibility of the method increases its versatility when applied to mission design scenarios. In actual design problems the solution provided by this method is in agreement with well-known optimized solutions. The fact that coast arcs are introduced naturally compensates some high-thrust peaks. In the presented example the mass fraction differs in only 2% when compared to the optimal solution.

ACKNOWLEDGEMENT

This work has been carried out at the Jet Propulsion Laboratory within the framework of the JVSRP program. It is part of the research project entitled "Dynamical Analysis, Advanced Orbit Propagation and Simulation of Complex Space Systems" (ESP2013-41634-P) supported by the Spanish Ministry of Economy and Competitiveness. Authors thank the Spanish Government for its support and J. Roa especially thanks "La Caixa" for his doctoral fellowship. They are indebted to J. Senent for motivating this work, and wish to thank A. Petropoulos, N. Arora and J. Sims for their advice.

REFERENCES

[1] R. H. Bacon, "Logarithmic Spiral: An Ideal Trajectory for the Interplanetary Vehicle with Engines of Low Sustained Thrust," *Am J Phys*, Vol. 27, No. 3, 1959, pp. 164–165, 10.1119/1.1934788.

[2] T. Tsu, "Interplanetary travel by solar sail," *ARSJ*, Vol. 29, No. 6, 1959, pp. 422–427, 10.2514/8.4791.

[3] A. E. Petropoulos and J. M. Longuski, "Shape-based algorithm for the automated design of low-thrust, gravity assist trajectories," *J Spacecraft Rockets*, Vol. 41, No. 5, 2004, pp. 787–796, 10.2514/1.13095.

[4] P. D. Pascale and M. Vasile, "Preliminary design of low-thrust multiple gravity-assist trajectories," *J Spacecraft Rockets*, Vol. 43, No. 5, 2006, pp. 1065–1076, 10.2514/1.19646.

[5] D. Gondelach and R. Noomen, "Hodographic-Shaping Method for Low-Thrust Interplanetary Trajectory Design," *J Spacecraft Rockets*, Vol. 52, No. 3, 2015, pp. 728–738, 10.2514/1.A32991.

[6] H. Tsien, "Take-off from satellite orbit," *J Am Rocket Soc*, Vol. 23, No. 4, 1953, pp. 233–236.

[7] D. Izzo and F. Biscani, "Explicit Solution to the Constant Radial Acceleration Problem," *J Guid Control Dynam*, Vol. 38, No. 4, 2015, pp. 733–739, 10.2514/1.G000116.

[8] H. Urrutxua, D. Morante, M. Sanjurjo-Rivo, and J. Peláez, "DROMO formulation for planar motion: solution to the Tsien problem," *Celest Mech Dyn Astr*, Vol. 122, June 2015, pp. 143–168.

[9] J. Peláez, J. M. Hedo, and P. R. d. Andrés, "A special perturbation method in Orbital Dynamics," *Celest Mech Dyn Astr*, Vol. 97, No. 2, 2007, pp. 131–150, 10.1007/s10569-006-9056-3.

[10] J. Roa, M. Sanjurjo-Rivo, and J. Peláez, "Singularities in Dromo formulation. Analysis of deep flybys," *Adv Space Res*, Vol. 56, August 2015, pp. 569–581, 10.1016/j.asr.2015.03.019.

[11] J. Roa and J. Peláez, "Orbit propagation in Minkowskian geometry," *Celest Mech Dyn Astr*, Vol. 123, 2015, pp. 13–43, 10.1007/s10569-015-9627-2.

[12] M. R. Akella and R. A. Broucke, "Anatomy of the constant radial thrust problem," *J Guid Control Dynam*, Vol. 25, No. 3, 2002, pp. 563–570, 10.2514/2.4917.

[13] J. Roa and J. Peláez, "Generalized logarithmic spirals for low-thrust trajectory design," *AAS/AIAA Astrodynamics Specialist Conference*, No. 15-729, 2015.

[14] J. Roa, J. Peláez, and J. Senent, "Generalized logarithmic spirals for low-thrust trajectory design," *J Guid Control Dynam*, 2015.

[15] C. G. Sauer, "Solar electric performance for Medlite and Delta Class planetary missions," *American Astronautical Society*, 1997, pp. AAS Paper 97–926.